Journal of Alloys and Compounds 504S (2010) S251–S255

Contents lists available at ScienceDirect

Journal of Alloys and Compounds

journal homepage: www.elsevier.com/locate/jallcom

Microstructure evolution of $Zr_{60}Al_{15}Ni_{25}$ bulk metallic glass subjected to rolling at room temperature

Z.J. Yan*, J. Yan, L.F. Tuo, Y. Hu, S.E. Dang

School of Materials Science and Engineering, Taiyuan University of Science and Technology, Taiyuan, 030024, PR China

ARTICLE INFO

Article history:
Received 18 July 2009
Received in revised form 16 April 2010
Accepted 19 April 2010
Available online 15 May 2010

Keywords:
Metallic glasses
Plastic deformation
Shear bands
Crystallization
Free volume

ABSTRACT

The microstructure evolution of $Zr_{60}Al_{15}Ni_{25}$ bulk metallic glass during rolling at room temperature has been investigated by differential scanning calorimetry (DSC) and high-resolution transmission electron microscopy (HRTEM). The released heat due to the structural relaxation before glass transition in the DSC curves indicates a two-state characteristic of atomic movement during rolling of the metallic glass, as modeled in the free volume model and shear-transformation-zone theory. The HRTEM images show that nanocrystallization preferentially occurs in the transition regions between the shear bands and the undeformed amorphous matrix. The gradient content distribution of excess free volume along the width of a shear band is conceived, based on which the variation of viscosity within a shear band is analyzed. Then the mechanism of deformation-induced crystallization is discussed within the frame of viscous flow.

1. Introduction

Bulk metallic glasses (BMGs) possess higher strength, hardness, elastic deformation limit and low elastic module compared to traditional metals, which promise potential application in engineering [1]. At low temperatures and high strain rates, plastic deformation in BMGs behaves in an inhomogeneous mode, namely, the deformation is highly localized in the shear bands, leading to a catastrophic failure [2]. As a result, much attention has been paid on the plastic deformation and fracture mechanism of metallic glasses. Previous works show that partial crystallization or phase separation occurs in deformed metallic glasses [3–6]. Based on the melting droplets and vein patterns on fracture surfaces, it is speculated that the material near the fracture would be adiabatically heated above the melting point when cracks rapidly propagate, and such considerable temperature rise results in crystallization [6–9]. However, it is estimated that the temperature rise within the shear bands before facture is much lower, and even is lower than the glass transition temperature (T_g) [10]. In fact, crystallization and phase separation occur during rolling of $Cu_{60}Zr_{20}Ti_{20}$ BMG at the temperature of 150 K [5,6], under which the considerable temperature rise is excluded.

Using the NTP (i.e., the number of atoms, temperature and pressure are constant) ensemble molecular dynamics simulation, Tarumi et al. have studied the structure changes during shear deformation in a Ni amorphous metal and found that the precipitated crystalline phase has an orientation relationship, namely, the shear direction and a (1 1 1) plane are parallel [11], which is consistent with the experimental studies on a Ni–P amorphous alloy [12,13]. As we know, a crystal induced by thermal diffusion should have a random orientation relationship. In this sense, the driving origin of deformation-induced crystallization in a metallic glass is not as simple as adiabatic heating.

The microstructure of a metallic glass during inhomogeneous plastic deformation varies within the shear bands, with the amorphous matrix being elastic deformation [3–7]. In the previous works, we have reported the two-state characteristic of atomic movement during rolling of the $Zr_{60}Al_{15}Ni_{25}$ metallic glass at room temperature based on the results of XRD and DSC [14]. Within a shear band, the excess free volume induced by shear stress distributes heterogeneously, which considerably influences the microstructure of a metallic glass [5–9]. In the present work, we further investigate the microstructure evolution based on the variation of free volume and the crystallization behaviors in the shear band zones to approach the understanding of the mechanism of deformation-induced crystallization.

2. Experimental procedure

An alloy ingot with nominal composition of $Zr_{60}Al_{15}Ni_{25}$ (atomic percent) was prepared by arc melting the mixture of pure metals Zr (99.9 wt%), Al (99.99 wt%) and Ni (99.95 wt%) in a water-cooled copper crucible under titanium-gettered argon atmosphere. The ingot was remelted four times to ensure its compositional homogeneity. Specimens with a cross-section of 1 mm × 10 mm and length about 50 mm were produced from the ingot by suction casting in a copper mold. Amorphous nature of the as-cast specimens was identified by X-ray diffraction (XRD) using Cu-K_α radiation.

* Corresponding author.
E-mail address: yanzhijie74@sohu.com (Z.J. Yan).

0925-8388/$ – see front matter © 2010 Elsevier B.V. All rights reserved.
doi:10.1016/j.jallcom.2010.04.130

The as-cast specimens were cut into small bars with a cross-section of 1 mm × 2 mm and length of 10 mm for subsequent rolling. Both the opposite wider surfaces of bar samples were mechanically polished to make them parallel to each other prior to rolling experiments. These bars, covered by two steel foils, were rolled at room temperature to the desired thickness in a twin-roller apparatus with a roller diameter of 120 mm. The reduction of space between the rollers per pass is no more than 1 μm. Under this status, the strain rates are controlled to be about 10^{-4}–10^{-3} s^{-1}. The deformation degree was evaluated by the reduction in thickness, i.e., $\varepsilon = (h_0 - h)/h_0$, where h_0 and h stood for the specimen thickness of as-cast and as-rolled specimens, respectively. The maximum ε of 95% was obtained in the present work.

Thermal analyses were performed in a Perkin–Elmer Pyris Diamond differential scanning calorimeter (DSC) at a scanning rate of 20 K/min under flow of high purity argon. The microstructures of the rolled samples were investigated by XRD and high-resolution transmission electron microscopy (HRTEM) under an accelerating voltage of 200 kV (JEOL JEM-2100 F). The TEM foils with a diameter of 3 mm were prepared using a twin-jet thinning electropolisher in a solution of 5% (vol.%) perchloric acid and 95% ethanol at 243 K. The TEM specimens were observed immediately after the preparation since they readily oxidized upon exposure to air atmosphere.

3. Results

The as-cast $Zr_{60}Al_{15}Ni_{25}$ specimens have been verified to be fully amorphous by XRD and HRTEM. The XRD patterns of as-cast and rolled specimens have been shown in our previous work [14]. Besides the broad diffraction peaks, no obvious signals for crystalline phases were detected in the XRD patterns. By fitting the broad diffraction peaks located at $2\theta \approx 37^\circ$ in the XRD patterns using Lorentz line profiles, the variation of values of full width at the half maximum (FWHM) with ε is not monotonic, indicating the two-state characteristic of deformation [14].

Free volume is a critical factor in evaluation of the microstructure of a metallic glass. But, it is difficult to measure the absolute content of free volume in a BMG quantitatively. Van den Buekel and co-workers have found that the released heat (E_r) due to structure relaxation before glass transition in a DSC curve at a constant scanning rate is proportional to the change of free volume (ΔV_f) [15,16]. Based on this, we can characterize the relative comparison of free volume accumulated in a metallic glass. Fig. 1(a) shows the DSC curves of the as-cast and some rolled specimens recorded at the scanning rate of 20 K/min. All the DSC traces show an endothermic event, which is the characteristic of glass transition, followed by a single exothermic event corresponding to the crystallization process. These DSC curves are expressed in the relative change of the apparent specific heat $\Delta C_p = C_P(T) - C_P$ (323 K) (Fig. 1(b) and (c)), where C_P (323 K) and $C_P(T)$ are the apparent specific heat at the temperatures 323 K and T, respectively.

Fig. 2(a) shows the variation of onset temperature (T_r) of structure relaxation with ε. T_r dramatically decreases from 465.3 K to 410.1 K as ε increases from 0% (as-cast) to 10%, and increases to 420.3 K at ε = 20%. Then, it fluctuates near 400.0 K as ε = 30–95%. The results show that the structure relaxation is considerably facilitated due to rolling, which is consistent with the previous work [17]. This is possibly attributed to the increase in free volume, which provides a larger driving force for relaxation. The values of E_r are calculated from the curves in Fig. 1(b) and (c) and shown in Fig. 2(b). The values of E_r of rolled specimens considerably fluctuate, with largest value of 34.9 J/g at ε = 70% and smallest value of 11.2 J/g at ε = 50%. The value of E_r of as-cast metallic glass is 7.5 J/g. A higher value of E_r indicates more abundant free volume and a more disordered atomic configuration. It is obvious that the free volume substantially increases due to rolling, which is in good agreement with previous works [18–20].

The HRTEM image of specimen with ε of 20% is shown in Fig. 3(a). The deformation of $Zr_{60}Al_{15}Ni_{25}$ metallic glass subjected to rolling under the present conditions behaves as an inhomogeneous mode, which is verified by the formation of localized shear bands (Fig. 3(a)). Shear bands appear bright, as they are thinner than the undeformed matrix due to less resistance to chemical attack during electrolytic thinning [18]. Between the bright center region of shear band (marked B) and the amorphous matrix, there is a moderate contrast field (i.e., transition regions marked A) in the HRTEM image. Fig. 3(b) and (c) shows the SAED patterns of shear bands and matrix in the specimens with ε of 20%, respectively. Fig. 3(d) shows the SAED pattern of shear band at ε of 40%. All the patterns exhibit diffusion halos without diffraction spots, showing amorphous nature. However, there exist differences among the three SAED halos, indicating the structure changes of the shear bands with increasing of deformation degree.

Many nanocrystals with size of about 5–10 nm are found in the transition than center regions of shear bands in the rolled spec-

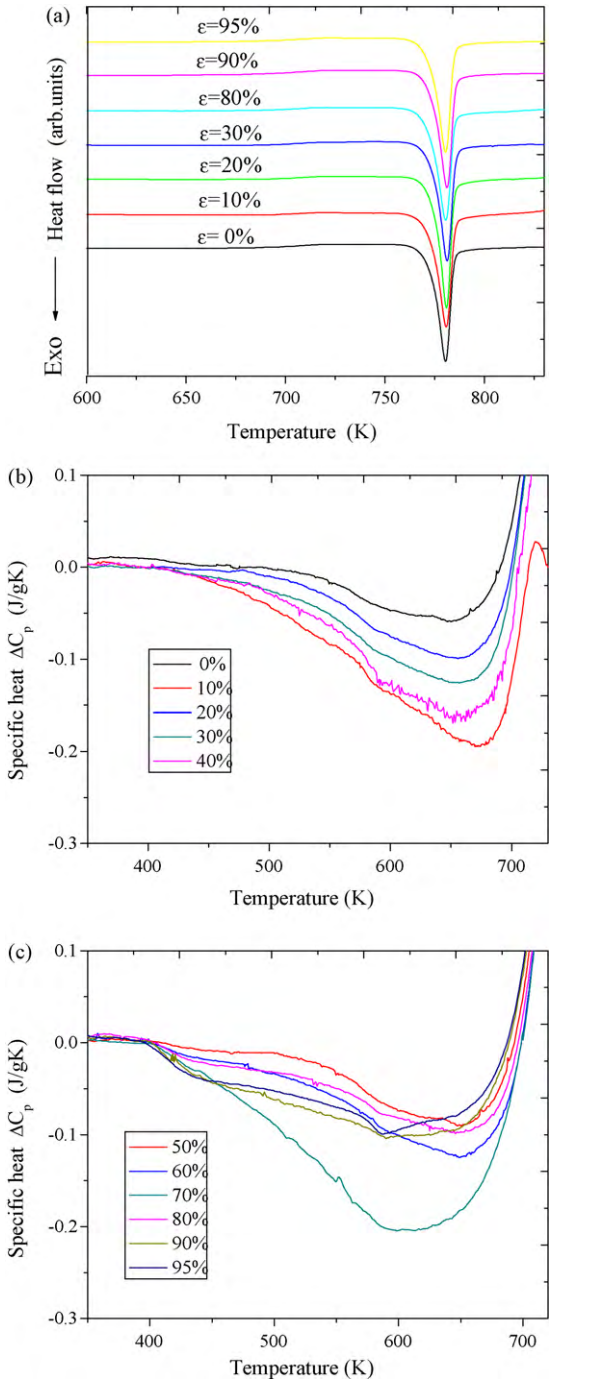

Fig. 1. DSC curves of the as-cast and some rolled $Zr_{60}Al_{15}Ni_{25}$ specimens with different ε at the heating rate of 20 K/min (a) and the corresponding relatively specific heat ΔC_p curves before glass transition ((b) and (c)).

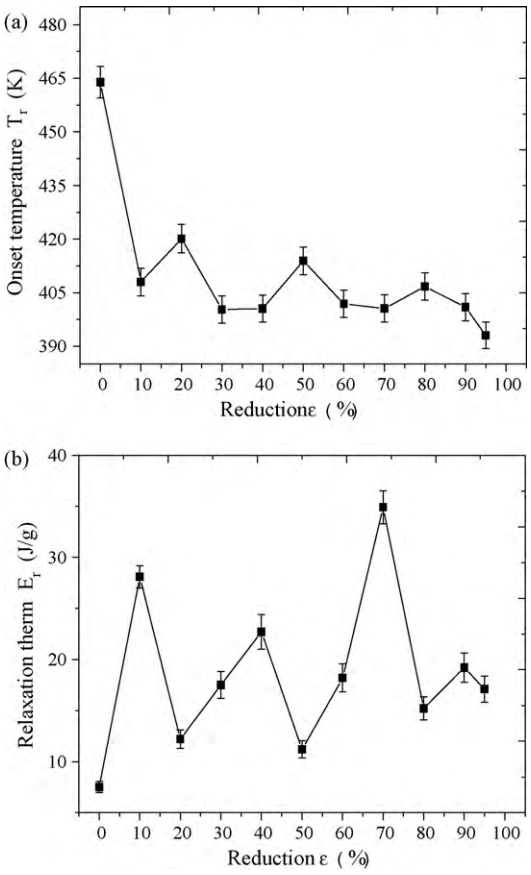

Fig. 2. Onset temperatures T_r of structure relaxation (a) and the corresponding released heat E_r of the as-cast and some rolled specimens (b).

imens with ε of 80%, marked with the ellipses in Fig. 4(a). The corresponding SAED pattern of the marked regions is shown in Fig. 4(b), showing obvious diffraction characteristic of polycrystals. The *d*-spacing evaluated from the observed ring pattern is about 0.19 nm. However, the diffusion halo of undeformed matrix (the insert of Fig. 4(a)) indicates its amorphous nature.

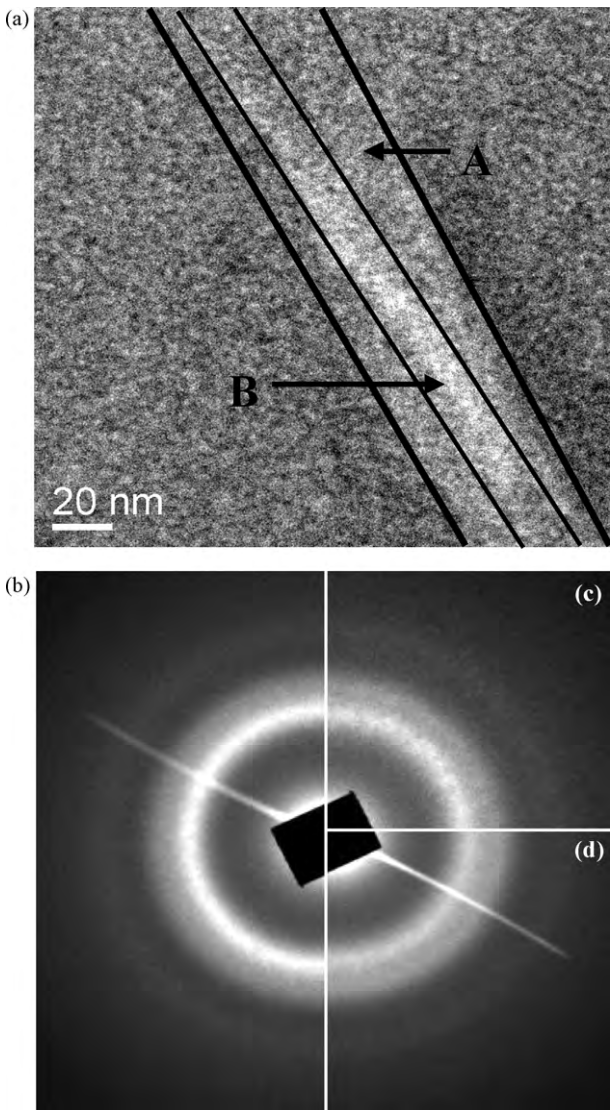

Fig. 3. HRTEM image of the shear band in $Zr_{60}Al_{15}Ni_{25}$ specimens with ε of 20% (a), and the SAED patterns of shear band with ε of 20% (b), the amorphous matrix (c), and the shear band in specimens with ε of 40% (d).

4. Discussion

At temperatures far below the temperature T_g, as the mechanical force loaded on a metallic glass exceeds the yield strength, some atoms are first driven by the shear stress to jump. As a result, additional volume defects (e.g., free volume, nano-voids) are introduced, and the local regions with higher energy appear. Extension of these regions along the maximum shear stress direction leads to the so-called shear bands. The strain in the shear bands is very high, while that in the amorphous matrix is about zero [2,3]. It is the propagation of shear bands, excess free volume, nano-voids and short-range orders that result in the complication of microstructure evolution during plastic deformation.

The non-monotonic variation of the values of E_r with ε further indicates a two-state characteristic of atomic movement subjected to rolling, namely, the competition between "forward" jumps or STZ operations with "backward" ones [4,21–23]. These behaviors have implications for the rheology of flowing glass, as well as cyclic deformation. This can be explained within the frames of free volume model (FVM) and shear-transformation-zone (STZ) theory. The viscosity in the shear bands substantially decreases due to the increase in excess free volume, and the atomic diffusion enhances. Diffusion controlled reordering leads to annihilation of free volume and the shear-induced disordering produces more free volume [4,24,25]. When the free volume exceeds the critical value, three dimensional nano-voids form as a result of coalescence of the excess free volume [26]. Based on the STZ theory, flow dilatation and flow contraction result in the ordering and disordering, respectively [4,21–25]. Shear bands were compressed by the amorphous matrix due to the substantial accumulation of excess free volume during shear transformation flow. Contraction and orderly arraying occur in shear transformation zone due to the compression effect, which has been certificated by molecular dynamics simulations [27]. Stress concentration occurs at the sites of flow defects during shear transformation. Therefore, nano-voids (with size about 3–6 atoms) may be "cut" into several smaller volume defects when STZ units operate through the defects. The repeated "cutting" effect results in the degradation of nano-voids into dispersed free volume, and therefore, disordering. The final microstructures of shear bands are the net result of two competing processes, viz., disordering and reordering.

Free-volume models for the kinetics of plastic flow in metallic glasses have predicted the creation of excess free volume in shear bands during plastic deformation. Previous works have indicated that much additional excess free volume accumulates in the shear

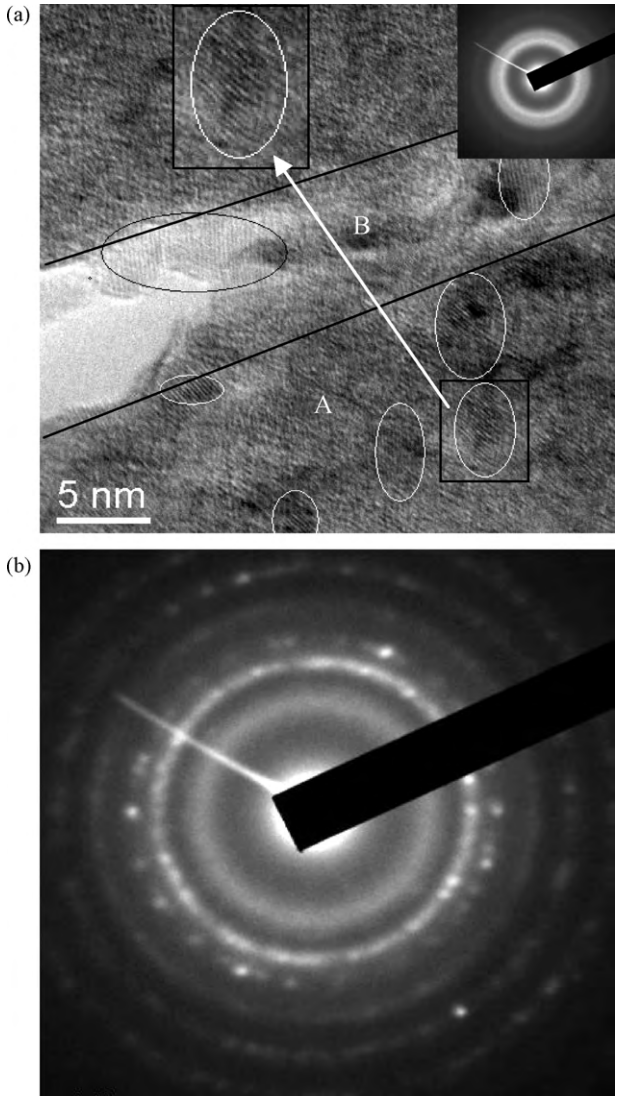

Fig. 4. HRTEM image near one shear band in the specimens with $\varepsilon = 80\%$ (a), and the corresponding SAED pattern of the ellipse region (b), showing polycrystalline characteristic. The insert in the HRTEM image (a) are the SAED pattern of matrix and a local magnified crystallized area.

bands [18–20]. The DSC data in the present work further verify the considerable increase in free volume due to rolling. The HRTEM images show that the content of excess free volume accommodated in one shear band shows a gradient distribution along its width orientation. The number of electrons that penetrate the objective lens and arrive at the image plane can be expressed as [28]:

$$n = n_0 \exp(-N\sigma x) \tag{1}$$

where $N = N_0/A$, A is the average atoms weight, and N_0 the Avogadro constant, and σ a constant related to atomic number; $x = \rho t$, ρ and t are the density and thickness of samples, respectively. Accordingly, the HRTEM image contrast is controlled by the density and thickness of samples. The density of one shear band is influenced by its excess free volume. Furthermore, the regions with higher content of free volume are easier to be electrochemically polished [18]. Based on the discussion above, the image contrast reflects the relative variation of the content of free volume, namely, the brighter contrast corresponds to the higher content of free volume. Fig. 5(a) and (b) is the schematic illustration of the distribution of excess free volume and viscosity along the width orientation of one shear band, respectively.

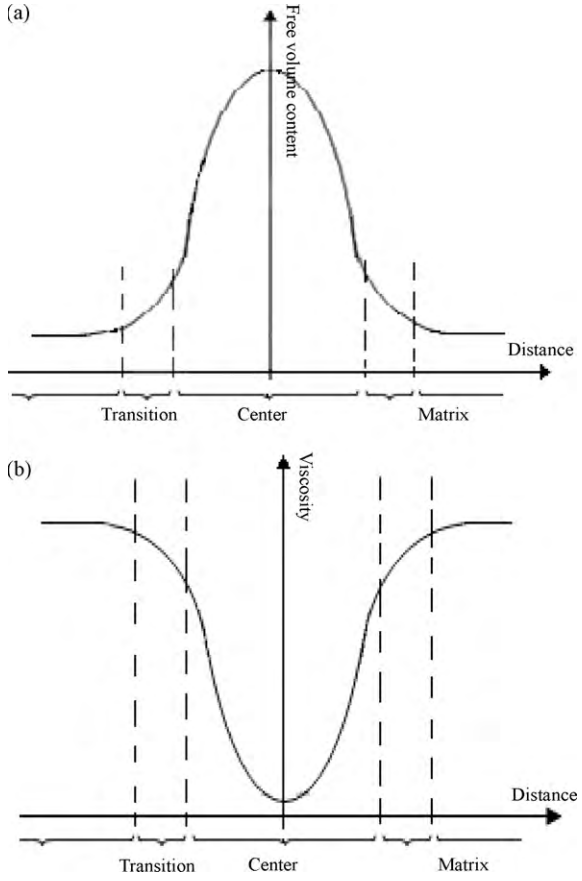

Fig. 5. Schematic illustration of the free volume (a) and viscosity (b) in one shear band.

Considering the lower viscosity, we take the deformation in shear bands as homogeneous plastic flow and the compression components to shear bands during rolling can be hold as hydrostatic pressure. Ye and co-workers have investigated the influence of hydrostatic pressure on the deformation-induced crystallization behaviors in metallic glasses [29–33]. For the homogeneous nucleation of a spherical crystallite with a radius (r) in an amorphous matrix, the relationship describing the change in the energy barrier for nucleation (ΔG^*) needed to form a critical sized nucleus associated with the hydrostatic pressure (P) can be expressed as [29,30]:

$$\left(\frac{\partial \Delta G^*}{\partial P}\right)_T = -\frac{64}{3}\pi\gamma^3 \frac{\Delta V_m}{(\Delta G_m + E_e + P\Delta V_m)^3} V_m^{c2} \tag{2}$$

where γ is the interfacial free energy between the crystalline and the amorphous phases, ΔG_m is the molar free energy change for an amorphous-to-crystalline phase transformation. E_e is the elastic energy induced by a volume change during the phase transformation in the solid state, V_m^c is the molar volume of the crystalline phase, and ΔV_m is the molar volume change associated with the formation of a crystalline nucleus.

In the case of the amorphous-to-crystalline transformation, the values for ΔG_m and ΔV_m are both negative, and as a result, E_e in this phase transformation is rather low [29,33]. Therefore, the value of $(\partial(\Delta G^*)/\partial P)_T$ is also negative, indicating that ΔG^* decreases with the increasing of hydrostatic pressure, suggesting that the application of hydrostatic pressure enhances the precipitation of nanocrystallites in the amorphous matrix. The transition regions of shear bands are compressed due to viscous dilation of the shear band and the restriction of matrix, leading to the decline of energy

barrier for nucleation (ΔG^*). As a result, nucleation prefers to occur in these transition regions. As the HRTEM images (Fig. 4(a)) show, nanocrystals highly localize in the transition regions. The crystalline/amorphous grain boundaries may drain out excess free volume during the crystal nucleation and growth, during which these free volume coalescence into nano-voids. In fact, Falk et al. have found that short-range orders accompany the nano-voids by molecular dynamics simulations [25]. Jiang and Atzom have also detected more nano-voids in the transition regions than the center of shear bands in nanocrystalline/amorphous $Al_{90}Fe_5Gd_5$ composites produced by rolling [34]. All these results suggest that nucleation during deformation-induced crystallization occurs in the transition regions of shear bands, which is consistent with our findings.

With higher excess free volume, the center regions of shear band have lower viscosity and larger shear strain than the transition regions, resulting in more severe viscous flow, indicating a more disordering effect. Furthermore, the energy barrier for nucleation increases due to its flow dilation. Therefore, the nucleation in the center regions of shear bands is considerably suppressed. This is also consistent with the previous report that nanocrystals preferentially precipitate in the compressive regions during the bending of $Al_{90}Fe_5Gd_5$ amorphous alloy [35].

5. Conclusions

The microstructure evolution of $Zr_{60}Al_{15}Ni_{25}$ bulk metallic glass during rolling at room temperature is investigated. The values of E_r non-monotonically vary with deformation degree, indicating that the atomic movement exhibits a two-state characteristic during plastic deformation. The final microstructure is the net result of two competing processes, viz., disordering and ordering. The HRTEM images show that the deformation-induced nanocrystallization preferentially occurs in the transition regions between the center of shear bands and the undeformed amorphous matrix, which is attributed to the compression effect duet to viscous dilation of the shear bands and the restriction of undeformed matrix. Based on the HRTEM images, a gradient content distribution of excess free volume along the width of a shear band is conceived, with the highest content of free volume in the center of the shear band. The present work is helpful to understand the mechanism of deformation-induced crystallization of amorphous alloys.

Acknowledgements

This project was financially supported by the National Natural Science Foundation of China (grant no. 50804032), the Natural Science Foundation of Shanxi Province, China (grant no. 2008011046), the Key Technologies R & D Program of Shanxi Province, China (20080321036).

References

[1] W.H. Wang, C. Dong, C.H. Shek, Mater. Sci. Eng. R 44 (2004) 45.
[2] F. Spaepen, Acta Metall. 25 (1977) 407.
[3] H. Chen, Y. He, G.J. Shiflet, Nature (London) 367 (1994) 541.
[4] C.A. Schuh, T.C. Hufnagel, U. Ramamurty, Acta Mater. 55 (2007) 4067.
[5] Q.P. Cao, J.F. Li, Y. Hu, A. Horsewell, Mater. Sci. Eng. A 457 (2007) 94.
[6] Q.P. Cao, J.F. Li, Y.H. Zhou, Appl. Phys. Lett. 86 (2005) 081913.
[7] H.A. Bruck, A.J. Rosakis, W.L. Johnson, J. Mater. Res. 11 (1996) 503.
[8] C.T. Liu, L. Heatherly, D.S. Easton, A. Inoue, Metall. Mater. Trans. A 29 (1998) 1811.
[9] H.J. Chang, D.H. Kim, Y.M. Kim, Y.J. Kim, K. Chattopadhyay, Scripta Mater. 55 (2006) 509.
[10] W.J. Wright, R. Saha, W.D. Nix, Mater. Trans. 42 (2001) 642.
[11] R. Tarumi, A. Ogura, M. Shimojo, K. Takashima, Y. Higo, Jpn. J. Appl. Phys. 39 (2000) L611.
[12] A. Ogura, M. Sato, R. Tarumi, M. Shimojo, K. Takashima, Mater. Res. Soc. Symp. 634 (2001) B1.10.
[13] A. Ogura, R. Tarumi, M. Shimojo, T. Kakashima, Y. Higo, Appl. Phys. Lett. 79 (2001) 1042.
[14] S.E. Dang, G. Zhang, Z.Y. Li, Z.J. Yan, Y.T. Li, W. Liang, J. Alloy Compd. 479 (2009) L15.
[15] A. Van den Beukel, J. Sietsma, Acta Metall. 38 (1990) 383.
[16] G.P. Debenedetti, F.H. Stillinger, Nature 410 (2001) 259.
[17] B.P. Kanungo, M.J. Lambert, K.M. Flores, Mater. Res. Soc. Symp. 806 (2004) MM7.1.1.
[18] C.A. Pampillo, Scripta Metall. 6 (1972) 915.
[19] K. Hajlaoui, T. Benameur, G. Vaughan, A.R. Yavari, Scripta Mater. 51 (2004) 843.
[20] K.M. Flores, D. Suh, R.H. Dauskardt, J. Mater. Res. 17 (2002) 1153.
[21] M.L. Falk, Y.F. Shi, Mater. Res. Soc. Symp. Proc. 754 (2003) CC6.20.1.
[22] P.D. Hey, J. Sietsma, A. Van den Beukel, Acta Mater. 46 (1998) 5873.
[23] K.M. Flores, R.H. Dauskardt, Acta Mater. 49 (2001) 2527.
[24] F. Faupel, Rev. Mod. Phys. 75 (2003) 237.
[25] A.S. Argon, Acta Metall. 27 (1979) 47.
[26] W.J. Wright, T.C. Hufnagel, W.D. Nix, J. Appl. Phys. 93 (2003) 1432.
[27] M.L. Falk, J.S. Langer, Phys. Rev. E 57 (1977) 7192.
[28] J. Edington, Practical Electron Microscopy in Materials Science, Philips Technical Library, Eindhoven, 1975, p. 57.
[29] S.W. Lee, M.Y. Huh, S.W. Chae, J.C. Lee, Scripta Mater. 54 (2006) 1439.
[30] S.W. Lee, M.Y. Huh, E. Feury, J.C. Lee, Acta Mater. 54 (2006) 349.
[31] F. Ye, K. Lu, Acta Mater. 47 (1999) 2449.
[32] F. Ye, K. Lu, Phys. Rev. B 60 (1999) 7018.
[33] Y.X. Zhuang, J.Z. Jiang, T.J. Zhou, H. Rasmussen, L. Gerward, M. Mezouar, et al., Appl. Phys. Lett. 77 (2000) 4133.
[34] W.H. Jiang, M. Atzom, Appl. Phys. Lett. 86 (2005) 151916.
[35] W.H. Jiang, M. Atzmon, Acta Mater. 51 (2003) 4095.